Eur. Phys. J. D **31**, 403–408 (2004)
DOI: 10.1140/epjd/e2004-00152-9

THE EUROPEAN PHYSICAL JOURNAL D

Photo-dissociation of Cold MgH^+ ions

Towards rotational temperature measurements and controlled dissociation

A. Bertelsen[1], I.S. Vogelius[1], S. Jørgensen[1,2], R. Kosloff[2], and M. Drewsen[1,a]

[1] QUANTOP, Danish National Research Foundation Center for Quantum Optics, Department of Physics and Astronomy, University of Aarhus, 8000 Aarhus C, Denmark
[2] The Fritz Haber Research Center for Molecular Dynamics, Hebrew University, Jerusalem 91904, Israel

Received 26 July 2004 / Received in final form 30 August 2004
Published online 23 November 2004 –

Abstract. Molecular ions sympathetically cooled into a Coulomb crystal by laser cooled atomic ions represent in many ways an ideal target for molecular physics studies due to achievable low translational temperatures (∼10 mK) and strong spatial localization (∼1 μm). In particular, in experiments with focused laser beams, both these features can be extremely useful. Here, we present results from experiments on photo-dissociation of MgH^+ ions in Coulomb crystals, and discuss possible avenues for using such processes for rotational temperature measurements as well as for manipulating the branching ratio of the dissociation channels $Mg+H^+$ and Mg^++H through intensity and frequency control of the laser beams involved.

PACS. 33.80.Ps Optical cooling of molecules; trapping – 33.20.Vq Vibration-rotation analysis – 82.37.Vb Single molecule photochemistry – 82.53.Kp Coherent spectroscopy of atoms and molecules

1 Introduction

In recent years, significant efforts have been focused on cooling, trapping and otherwise controlling molecules in the gas phase. Since conventional laser coolings techniques applicable to atoms generally fail to work for molecules due to their complex internal level structure, the development of completely different approaches is necessary for cooling molecules. For neutral molecules such new techniques include electrostatic deceleration (and trapping) [1,2], buffer gas loading of magnetic traps [3–5], photo-association in ultra-cold atomic gases [6], and most recently the creation of Bose-Einstein condensates of molecules using Feshbach resonances [7]. Other methods may be considered for molecular ions. For instance, the translational degrees of freedom of the molecules can be very efficiently cooled to the mK regime through interactions with simultaneously trapped and laser cooled atomic ions, independent on the electric or magnetic dipole moment of the molecules [8,9]. Although ionic molecules can be sympathetically cooled into Coulomb crystals, the population of the internal rovibrational states is expected to be determined by coupling to the blackbody radiation in the trap region for room temperature experiments ($T \approx 300$ K). However, since ionic molecules can be trapped without perturbation of the internal states for up to several minutes under UHV conditions, relatively simple schemes for cooling rotational degrees of freedom might as well be applied [10–12]. In order to obtain more accurate information on the internal rotational state distribution of ionic molecules before and after an internal cooling, it is necessary to develop a method to determine the internal state distribution. For the case of a single molecular ion sympathetically cooled by a single atomic ion [13] one can consider using a non-destructive shelving technique initially developed for atomic spectroscopy on a single ion sympathetically cooled by another ion to the ground state in the trapping potential [14]. However, for an ensemble of molecular ions, a destructive detection technique will be needed. In our effort to characterize the rotational distribution of MgH^+ molecules cooled into Coulomb crystals, we plan to apply a resonant two-photon dissociation scheme based on the $X^1\Sigma$ - $A^1\Sigma$ transition. In this article, we present the first experiment in this direction as well as consider the prospect for control of the branching ratio of the two possible dissociation channels, $Mg+H^+$ and Mg^++H.

2 Photo-dissociation scheme

The lowest singlet potentials for the MgH^+ molecule are presented in Figure 1 together with indication of the transitions driven by the applied laser fields in the experiments. The potential curves have been calculated with

[a] e-mail: drewsen@phys.au.dk

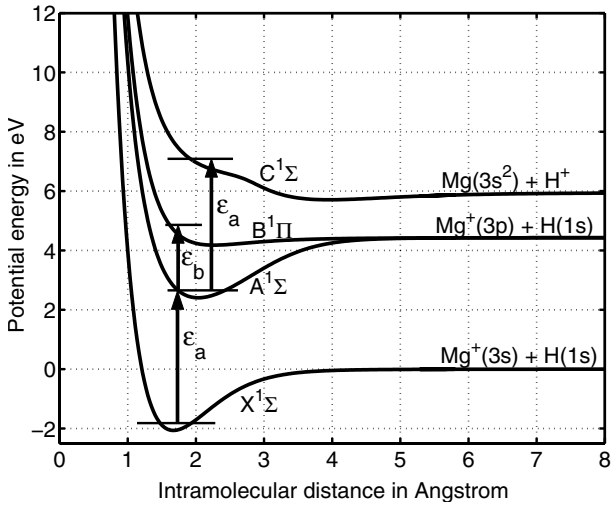

Fig. 1. Potential curves for the four lowest lying spin singlet electronic states of MgH^+ (details see Ref. [18]). The symbols ϵ_a and ϵ_b represents the electric fields of the laser used in the experiments.

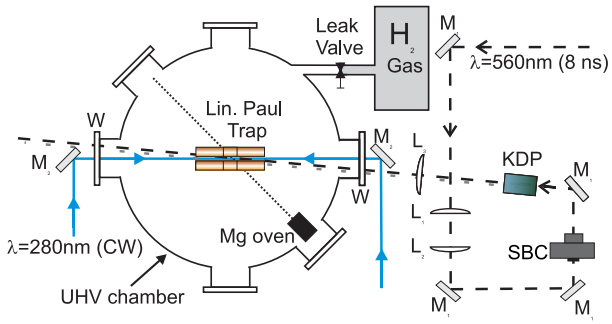

Fig. 2. Sketch of the experimental set-up. The letters on the figure have the following meanings: W is a window into the vacuum chamber, M_1 is a high-power mirror for 560 nm light, L_i's are lenses to shape the pulsed laser beam with L_3 being used to focus both the 560 nm and the 280 nm light to spot sizes of around 350 μm and 250 μm, respectively, KDP indicates the type of frequency doubling crystal used to produce the 280 nm light, SBC represents a Soleil-Babinet compensator used to optimize the polarization of the 560 nm light for frequency doubling, M_2 is a mirror for the laser cooling light at 280 nm. Not shown on the figure is a CCD-camera situated above the plane of the sketch which monitors fluorescence light from Mg^+ ions in the center of the linear Paul trap.

the state average multi-reference self consistent field (MCSCF) method [15,16] using the MOLPRO-package [17]. The computational details are presented in reference [18]. In the experiments presented here, the field ϵ_a is created by partially doubling the frequency of field ϵ_b, and hence their frequencies are always locked to each other. As shown, both of the two dissociation channels $Mg+H^+$ and Mg^++H are open when both fields are present.

3 Experimental technique

Figure 2 presents a sketch of the experimental set-up. The details of the linear Paul trap used in the experiments have been given in reference [19]. In short, it consists, like a standard quadrupole mass-filter, of four electrodes mounted so that by applying an rf voltage of the same phase to diagonal electrodes and with a phase shift of 180° with respect to the nearest electrodes, a near-ideal two-dimensional quadrupole field is created in the plane perpendicular to the direction defined by the length of the electrodes (the trap axis). Each electrode is sub-divided into three parts such that a positive dc voltage can be applied to the eight end-pieces. This dc voltage leads to static confinement of the ions along the trap axis. By crossing an atomic beam of magnesium with the ns-laser beams used in the dissociation experiments (see below) in the center of the trap, magnesium ions are produced through non-resonant photo-ionization processes. The laser beams applied to cool the magnesium ions to mK-temperatures are tuned to the $3s\ ^2S_{1/2}$–$3p\ ^2P_{3/2}$ transition around $\lambda = 280$ nm and propagate along the trap axis (see Fig. 2). These laser beams, focused to a spot size of around one millimeter, are derived from a frequency doubled CW dye laser with a typical output power of 20 mW.

The fluorescence light emitted during the cooling process is imaged onto an image-intensified CCD-camera. Simply from the spatial distribution of the light recorded in the CCD-images, one is able to deduce the thermodynamic state of the magnesium ion cloud [20,21]. When spatial ordered structures appear as an indication of the formation of Coulomb crystals, one can conclude that the temperature of the ion ensemble is below 100 mK [8].

In order to create the MgH^+ molecular ions, after loading and laser cooling of the magnesium ions into a Coulomb crystalline state, a gas of H_2 is leaked into the UHV chamber (background pressure: 1×10^{-10} Torr) at a partial pressure of $\approx 5\times10^{-10}$ Torr for a few minutes [8]. The number of molecular ions produced can continuously be monitored by observing the change in the structure of the resulting two-component Coulomb crystal [8,19] and hence controlled by closing the leak-valve after a certain time. It is important to note that when an ensemble of ions with identical charges is cooled into a Coulomb crystal in a linear Paul trap, the densities of the trapped ion species are constant and inversely proportional to the mass of the ions (see e.g. Ref. [22]). The outer boundary of an ion Coulomb crystal consisting of a single ion specie or ions species with nearly identical masses is spheroidal in shape [19,23], so it is possible to determine the total number of ions as well as the relative numbers of Mg^+ and MgH^+ ions [19] from images like those shown in Figure 3 just by measuring the spatial extension of the Coulomb crystal. Due to the physics of the trap (see, e.g., Ref. [19]), when both Mg^+ and MgH^+ ions are present, the Mg^+ ions always segregate near the trap axis in a nearly cylindrical symmetric volume with the heavier MgH^+ ions arranged radially outside such that the whole crystal has a nearly perfect spheroidal shape. An example of this is shown in Figure 3b.

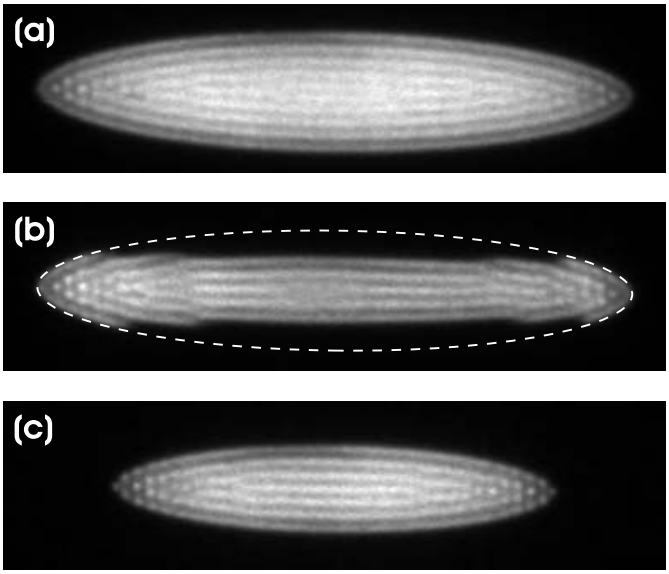

Fig. 3. (a) CCD-image of a Coulomb crystal with a total of a few thousand Mg^+ ions. (b) CCD-image after the ions in the Coulomb crystal in (a) have been reacting with H_2 molecules. Roughly half of the initial fluorescing Mg^+ ions have been converted into non-fluorescing MgH^+. The dashed lined ellipse illustrates the outer boundary of the Mg^+–MgH^+ Coulomb crystal. (C) CCD-image after the photo-dissociating laser beams have been present long enough that all MgH^+ ions have been dissociated. Nearly no non-fluorescing ions are left, proving that almost all MgH^+ molecules have been dissociated. The length of the CCD-images corresponds 950 μm.

Likewise, monitoring the changes in the structure of the Coulomb crystals when the dissociating laser beams are present can give information on the photo-dissociation processes. Mg^+ ions produced in the photo-dissociation processes will be trapped and start fluorescing, while H^+ ions will escape the trapping potential. Hence, we can from the CCD-images discriminate between the two dissociation channels depicted in Figure 1, by quantifying the volumes occupied by the Mg^+ and MgH^+ ions.

The light used to drive the photo-dissociation processes indicated in Figure 1, comes from a dye laser pumped by a pulsed frequency doubled Nd:YAG laser. The laser field ϵ_b around 560 nm is directly from the dye laser, while the laser field ϵ_a around 280 nm is created by partially frequency doubling the field ϵ_b just in front of the vacuum chamber as schematically shown in Figure 2. The pulsed dye laser system is operated with a repetition rate of 20 Hz with the pulse length of about 8 ns and a maximum pulse energy of about 10 mJ in the interaction zone. The frequency spectrum of each of these pulses is about 0.12 cm^{-1} in width, which is considerably narrower than the rotational splittings of the $X^1\Sigma(\nu = 0)$–$A^1\Sigma(\nu' = 0)$ transition of the MgH^+ ion, previously measured with an accuracy of 0.05 cm^{-1} [24]. Prior to the experiments, the dye laser has been absolute frequency calibrated to better than 0.1 cm^{-1} by optogalvanic spectroscopy on a series a neon lines in the neighborhood of 560 nm. In order to look for resonant effects in the photo-dissociation signal independent of the uncertainty in the transition energies indicated in reference [24], the uncertainty in the absolute calibration of the pulsed dye laser and possible frequency jitter, we have chosen to scan the laser frequency always at a rate of 1 Hz with a scan width that translates into a photon energy span of 0.95 cm^{-1} for the ϵ_a laser field. Reference will always be made to the center energy of that scan in the following.

4 Photo-dissociation results

In the photo-dissociation experiments discussed in this section, the laser field ϵ_a is detuned 1.0 cm^{-1} below the $X^1\Sigma(\nu = 0,\ J = 0)$–$A^1\Sigma(\nu' = 0,\ J = 1)$ transition according to reference [24].

The images presented in Figure 3 are the examples of the Coulomb crystals recorded before the reaction with H_2 molecules (a), after the reaction (b) and after the ns-laser beams have been present long enough for all MgH^+ ions to dissociate and only fluorescing Mg^+ ions to remain (c). In Figure 3b, the dashed lined ellipse indicates the boundary of the initial Coulomb crystal shown in Figure 3a. By recording sequences of CCD-images with the photo-dissociating laser beams present, the relative amounts of the Mg^+ and MgH^+ ions can be determined from the analysis of the shape and size of the Coulomb crystals in each image frame. In Figure 4, the amount of Mg^+ and MgH^+ ions relative to the initial number of Mg^+ ions before reactions are presented for two sets of laser intensities as function of the interaction time with the ns-lasers.

From both the low and high intensity experiments of Figure 4 it follows that the MgH^+ ions must dissociate nearly exclusively via the $C^1\Sigma$ potential curve into Mg and H^+ since the amount of Mg^+ ions does not change significantly during the interaction time. The main difference between Figures 4a and 4b is the time scale on which the dissociation takes place. The dissociation rate is observed to have a non-quadratic dependence on the intensity of the field ϵ_a. This indicates that even though the field ϵ_a is non-resonant with the $X^1\Sigma(\nu = 0,\ J = 0)$–$A^1\Sigma(\nu' = 0,\ J = 1)$ transition, the dissociation probably takes place via off-resonant excitation to the $A^1\Sigma$ potential curve. This non-quadratic dependence on the intensity has also been observed in other experiments not presented here. The apparent total lack of dissociation via the $B^1\Pi$ potential curve by the field ϵ_b is a bit surprising since it is energetically allowed. However, theoretical calculations as those presented in the following sub-section actually predict that dissociation through the $C^1\Sigma$ potential should be more favorable for the laser parameters used in the experiments.

In order to observe resonant effects in the dissociation signal, we have performed experiments with the laser field ϵ_a scanned around the resonance of the $X^1\Sigma(\nu = 0,\ J = 0)$–$A^1\Sigma(\nu' = 0,\ J = 1)$ and other rotational transitions. Though in a few experiments we have observed signs of resonant behavior in the sense that for some settings of the laser frequencies and intensities, dissociation via the

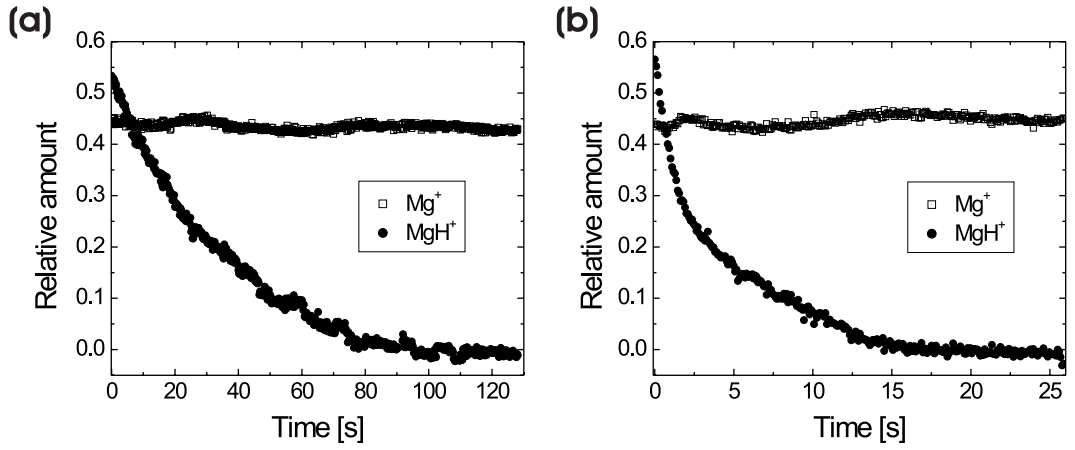

Fig. 4. The amount of Mg^+ and MgH^+ ions relative to the number of Mg^+ ions before the reactions as function of the interaction time with the dissociation laser beams. The data have been extracted from two different time-series of CCD-images recorded during the presence of the dissociation laser beams. (a) For these data the peak intensities of the two fields ϵ_a and ϵ_b were 1.6×10^7 W/cm^2 and 1.8×10^7 W/cm^2, respectively, and the frame rate of the CCD-camera 4.7 Hz. (b) Peak intensities of the two fields ϵ_a and ϵ_b were 4.3×10^7 W/cm^2 and 3.3×10^7 W/cm^2, respectively, and the frame rate 11.0 Hz. In both experiments, the laser field ϵ_a was detuned 1.0 cm^{-1} below the $X^1\Sigma(\nu = 0,\ J = 0)$–$A^1\Sigma(\nu' = 0,\ J = 1)$ resonance.

$B^1\Pi$ potential curve was observed, the control of the various experimental parameters such as laser beam profiles and overlap of the two laser fields at the right position in the trap region made it so-far impossible to quantify such results.

The next step in the direction of determining the rotational temperature will be to accumulate enough accurate experimental data for specific laser intensities and detunings, so that we can compare our results with theoretical models taking into account redistribution of the initial rotational population by molecules spontaneously decaying from the $A^1\Sigma$ states to the $X^1\Sigma$ states after laser excitation and by the blackbody radiation field present at about 300 K. From the observed rather slow time scale of dissociation in the first experiments, it is clear that both of these mechanisms have to be accounted for with the present available laser intensities.

5 Control of the dissociation branching ratio

In order to predict interesting parameter regimes for the two laser fields ϵ_a and ϵ_b, very recently we have set up a numerical simulation where the dynamics of the photodissociation is modeled by solving the time dependent Schrödinger equation

$$i\hbar\frac{\partial\tilde{\boldsymbol{\Psi}}(r,t)}{\partial t} = \tilde{\boldsymbol{H}}(r)\tilde{\boldsymbol{\Psi}}(r,t), \qquad (1)$$

with the state vector restricted to the four potential curves presented in Figure 1, and with the Hamiltonian including the couplings of the two laser fields ϵ_a and ϵ_b illustrated in the same figure.

The electric fields are assumed to be constant in amplitude, so that they may be written as

$$\epsilon_j(t) = \frac{1}{2}\,\bar{\epsilon}_j\,(e^{-i\omega_j t} + e^{i\omega_j t}), \quad j = a, b \qquad (2)$$

where ω_j and $\bar{\epsilon}_j$ are the carrier frequency and the electric field strength of the laser pulse ϵ_j, respectively. To eliminate the fast oscillating terms at optical frequencies, the rotating wave approximation is employed, such that the Hamiltonian can be written [25]

see equation below

where $\mu_{i,j}(r)$ is the position dependent electronic transition dipole moment between the electronic states i and j, which have been computed together with the potential energy curves in the electronic structure calculation. The operator $\boldsymbol{T} = -(1/2M_\mu)(\partial^2/\partial r^2)$ is the kinetic energy operator with M_μ being the reduced mass of the diatomic molecules and $\boldsymbol{V}_i(r)$ the potential energy for the state i. This model is simple. The rotational states are not described, with exception of $J = 0$. Nevertheless, the model may give us some guidelines as of interesting parameters for the frequencies and the intensities.

The initial wave function of the magnesium hydride ion, MgH^+, corresponds to an internal state of the ground electronic state, $X^1\Sigma$. In the simulations we used the

$$\tilde{\boldsymbol{H}}(r) = \begin{vmatrix} \boldsymbol{T} + \boldsymbol{V}_C(r) - \hbar\omega_a & 0 & \frac{1}{2}\boldsymbol{\mu}_{CA}(r)\bar{\epsilon}_a & 0 \\ 0 & \boldsymbol{T} + \boldsymbol{V}_B(r) - \hbar\omega_b & \frac{1}{2}\boldsymbol{\mu}_{BA}(r)\bar{\epsilon}_b & 0 \\ \frac{1}{2}\boldsymbol{\mu}_{AC}(r)\bar{\epsilon}_a & \frac{1}{2}\boldsymbol{\mu}_{AB}(r)\bar{\epsilon}_b & \boldsymbol{T} + \boldsymbol{V}_A(r) & \frac{1}{2}\boldsymbol{\mu}_{AX}(r)\bar{\epsilon}_a \\ 0 & 0 & \frac{1}{2}\boldsymbol{\mu}_{XA}(r)\bar{\epsilon}_a & \boldsymbol{T} + \boldsymbol{V}_X(r) + \hbar\omega_a \end{vmatrix}$$

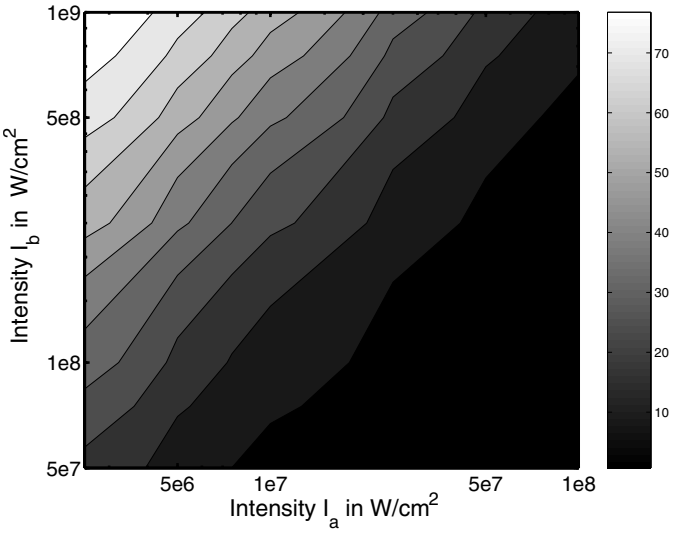

Fig. 5. The percentage of the total production yield in the dissociation channel, $Mg^+(3p)$+H$(1s)$, is shown as a function of the laser intensities. The initial state of the molecular system is represented by the lowest eigenstate on ground electronic state $X^1\Sigma(\nu = 0$ and $J = 0)$. The intensity is related to the electric field strength of the electric field by the expression $I = \epsilon_0\ c\ |\bar{\epsilon}|^2/2$, where c is the velocity of light and ϵ_0 is the electric constant.

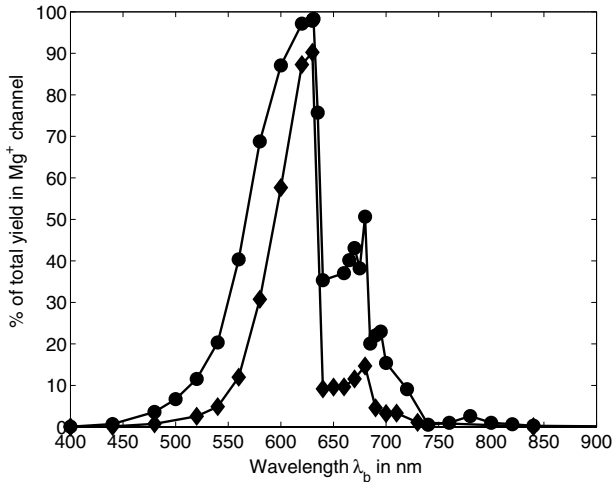

Fig. 6. The yield as a function of the wavelength, $\lambda_b = 2\pi c/\omega_b$, (given in nm) for set 1 the intensities of the two laser pulses are $I_a = 10^8$ W/cm^2 and $I_b = 10^9$ W/cm^2 whereas for set 2 they take the values $I_a = 5 \times 10^6$ W/cm^2 and $I_b = 2.5 \times 10^8$ W/cm^2.

lowest rovibrational state ($\nu = 0$ and $J = 0$). The initial wave function is propagated in time according to the time dependent Schrödinger equation using the Chebychev method [26]. The simulation time, or equivalent, the pulse duration of both laser fields, is 5 ps. This is much shorter than the pulse durations in the experiments presented above. This choice has deliberately been made to investigated the possibility of controlling the branching ratio of the two dissociation channels.

The dissociation yields are computed by integrating the flux of the wave functions for the two potential curves $B^1\Pi$ and $C^1\Sigma$ at $r = 7$ Å.

In Figure 5, the percentage of the total dissociation yield in the $Mg^+(3p)$+H$(1s)$ channel via the $B^1\Pi$ potential curves is shown as a function of the intensities of the two ps-pulses. In the simulations, we have used the experimental values of the laser frequencies, i.e. $\hbar\omega_b = \hbar\omega_a/2 = 4.4$ eV. As one might expect, we observe that the intensity of the two laser pulses can be used to control the branching ratio between the two dissociation channels. The intensity of the laser pulse enters in the off-diagonal elements of the Hamiltonian, which describes the population transfer between the two electronic states. As the intensity increases, the interaction between the molecular system and the laser pulse increases leading to large population transfer between the two curves. We observe, that the relative yield of producing magnesium ions increases as the intensity, I_b, increases due to large coupling between the $A^1\Sigma$ and $B^1\Pi$ electronic states. As the intensity, I_a, increases, the coupling between the two electronic states $A^1\Sigma$ and $C^1\Sigma$ increases leading to larger yield in the Mg$(3s^2)$+H^+ dissociation channel.

In Figure 6, the percentage of the total dissociation yield into the $Mg^+(3p)$+H$(1s)$ channel is shown as a function of the laser wavelength, λ_b, for two different sets of intensities of the lasers. In both calculations the wavelength of the laser field, ϵ_a, is chosen to be $\lambda_a = 280$ nm as in the experiment. Two peaks are observed in the spectrum, one around 630 nm and another one around 680 nm. At 630 nm the molecule is excited just above the threshold for dissociation on the $B^1\Pi$ potential energy curve. In the wavelength window (600–700 nm) the detuning $\Delta(r) = V_{B^1\Pi}(r) - V_{A^1\Sigma}(r) - \hbar\omega_b$ is almost zero around the equilibrium bond length for MgH^+ leading to a large population transfer to the $B^1\Pi$-state. Above 630 nm, part of the wave packet is excited below the threshold of the dissociation on the $B^1\Pi$ potential energy curve. Since the state is not an eigenstate, a fraction of the molecular ions would therefore dissociate.

Despite the large difference in time scales between the experimental and theoretical investigations, the results presented in Figures 5 and 6 are qualitatively in agreement with the experimental results in Figures 3 and 4. The above model shows that with the frequency, $\hbar\omega_b$ and the intensities (I_a and I_b) can be used to control the branching ratio of the dissociation channels. The present model is limited to the lowest rotational state $J = 0$. Future studies will extend the dynamical model to include other rotational states. This extention would lead to a comprehensive comparison with the experimental data.

6 Outlook

In the next series of experiments we will vary the intensity of the two fields ϵ_a and ϵ_b independently and look for similar control as seen in the theoretical calculations presented in Figure 5. By favouring the $Mg^+(3p)$+H$(1s)$ dissociation channel using this intensity control, we expect to get data

from which the rotation temperature of our sympathetically cooled molecular ions can be deduced. When this goal has been achieved, we will initiate experiments using incoherent light sources to manipulate the rotational distribution [10,11]. Calculations involving excitation from specific rovibrational levels in the ground state will be performed to study the state dependence of the dissociation processes. Also non-resonant contributions to the dissociation channels will be investigated, which might eventually lead to a full understanding of the observed non-resonant results of Figures 3 and 4. On a longer time scale other more complex coherent control mechanisms using, e.g., tailored ps-laser pulses will be investigated.

7 Conclusion

On the basis of the dissociation results presented in Figures 3 and 4, we are not yet able to deduce a precise value for an effective rotational temperature of the sympathetically cooled MgH^+ ions. However, by comparing experimental dissociation data with theoretical model simulations this should be possible in the near future. Theoretically, we have shown that the branching ratio between the two dissociation channels $Mg^+(3p)$+H and $Mg(3s^2)$+H^+ can be effectively controlled by varying either the intensity of the two lasers involved or the wavelength one of the lasers.

SJ is supported by the Carlsberg Foundation. This work has been supported by the European Union in the frame of the Cold Molecule TMR network under contract HPRN-CT-2002-00290 and Israel Science Foundation. The Fritz Haber Center is supported by the Minerva Gesellschaft für die Forschung GmbH München, Germany. MD acknowledges financial support from the Danish National Research Foundation.

References

1. H.L. Bethlem, G. Berden, G. Meijer, Phys. Rev. Lett. **83**, 1558 (1999)
2. H.L. Bethlem, G. Meijer, Int. Rev. Phys. Chem. **22**, 73 (2003)
3. J.D. Weinstein, R. deCarvalho, T. Guillet, B. Friedric, J.M. Doyle, Nature **395**, 148 (1998)
4. J.M. Doyle, B. Friedrich, Nature **401**, 749 (1999)
5. D. Egorov, D.J. Weinstein, D. Patterson, B. Friedrich, J.M. Doyle, Phys. Rev. A **63**, 030501(R) (2001)
6. A. Fioretti, D. Comparat, A. Crubellier, O. Dulieu, F. Masnou-Seeuws, P. Pillet, Phys. Rev. Lett. **80**, 4402 (1998)
7. M. Greiner, C.A. Regal, D.S. Jin, Nature **426**, 537 (2003)
8. K. Mølhave, M. Drewsen, Phys. Rev. A **62**, 011401(R) (2000)
9. S. Schiller, C. Lämmerzahl, Phys. Rev. A **68**, 053406 (2003)
10. I.S. Vogelius, L.B. Madsen, M. Drewsen, Phys. Rev. Lett. **89**, 173003 (2002)
11. I.S. Vogelius, L.B. Madsen, M. Drewsen, preprint `arXiv:physics/0406100`, Phys. Rev. A (to appear)
12. I.S. Vogelius, L.B. Madsen, M. Drewsen, preprint `arXiv:physics/0406082`, J. Phys. B (to appear)
13. M. Drewsen, A. Mortensen, R. Martinussen, P. Staanum, J.L. Sørensen, preprint `arXiv:physics/0406088`, Phys. Rev. Lett. (to appear)
14. D.J. Wineland, J.C. Bergquist, J.J. Bollinger, R.E. Drullinger, W.M. Itano, *Proc. of the 6th Symposium on Frequency Standards and Metrology* (World Scientific, New Jersey, 2002), p. 361
15. H.J. Werner, P.J. Knowles, J. Chem. Phys. **89**, 1007 (1988)
16. P.J. Knowles, H.J. Werner, J. Chem. Phys. **89**, 5803 (1988)
17. Werner, with contributions from R.D. Amos, Benhardsson, Berning, Celani, Cooper, Deegan, Dobbyn, Eckert, Hampel et al. MOLPRO: A package of ab initio programs, Version 2000.1
18. S. Jørgensen, R. Kosloff, A. Bertelsen, M. Drewsen, in preparation
19. M. Drewsen, I. Jensen, J. Lindballe, N. Nissen, R. Martinussen, A. Mortensen, P. Staanum, D. Voigt, Int. J. Mass Spec. **229**, 83 (2003)
20. M. Drewsen, C. Brodersen, L. Hornekær, J.S. Hangst, J.P. Schiffer, Phys. Rev. Lett. **81**, 2878 (1998)
21. L. Hornekær, M. Drewsen, Phys. Rev. A **66**, 013412 (2002)
22. L. Hornekær, N. Kjærgaard, A.M. Thommesen, M. Drewsen, Phys. Rev. Lett. **86** 1994 (2001)
23. A. Mortensen, J.J.T. Lindballe, I.S. Jensen, P. Staanum, D. Voigt, M. Drewsen, Phys. Rev. A **69**, 042502 (2004)
24. W.J. Balfour, Can. Jour. Phys. **50**, 1082 (1972)
25. A. Hammerich, R. Kosloff, M. Ratner, J. Chem. Phys. **97**, 6410 (1992)
26. R. Kosloff, Annu. Rev. Phys. Chem. **45**, 145 (1994)